

Statistical Modelling and Optimization of TIG Welding Process Parameters Using Taguchi's Method

S. Omprakasam^{1,*} – K. Marimuthu² – R. Raghu¹ – T. Velmurugan¹

¹Sri Ramakrishna Engineering College, Department of Mechanical Engineering, India

²Coimbatore Institute of Technology, Department of Mechanical Engineering, India

This current research focuses on optimizing the welding process parameters and penetration of 5052 alloys using a TIG welding process based on the Taguchi methods. Process parameters such as current, voltage, and speed with three different levels were taken to form the L27 orthogonal array using the design of experiments. Analysis of variance, signal-to-noise ratio analysis, and regression analysis were performed. The regression analysis indicated that the developed model has greater adequacy in predicting the reinforcement form factor (RFF), penetration shape factor (PSF) and hardness of the weld specimens. In addition, the optimized parametric condition for the welded specimen was found to be current, voltage, and speed of 140 A, 18 V, and 300 mm/min, respectively.

Keyword: TIG welding; aluminium; AA5052; hardness; RFF; PSF; Taguchi

Highlights

- The optimum conditions of current, voltage, and speed for attaining the maximum hardness of 145.3 HV while welding the AA5052 alloy have been determined.
- Among different parameters, current is found to have greater significance on RFF, PSF and hardness of the AA5052 alloy.
- The developed model is found to be adequate in correlating the process parameters with the RFF, PSF, and hardness of the welded specimens.
- Enhanced hardness is attained in the fusion zone of the welded AA5052 specimen.

0 INTRODUCTION

Modern fabrication industries join metallic materials through melting the base materials with the addition of filler materials. Welding has been a high-quality and cost-effective method for producing strong joints in several applications. Many conventional joining processes are used in the fabrication sectors. Among them, the tungsten inert gas (TIG) welding process was one of the popular conventional welding processes, primarily employed in the automobile, oil, gas pipeline, and container manufacturing sectors [1]. This TIG welding process was most commonly used in the joining of aluminium alloys. In comparison to aluminium alloys, aluminium AA5052 alloy possesses better weldability and excellent corrosion resistance to seawater and salt spray, making it ideal for marine applications [2]. The TIG welding process was preferred over other process for joining 5xxx alloys due to its ease and low cost [3]. Dengkui et al. [4] revealed that applying different geometric shapes to a material changes its mechanical properties; they characterized the weld joints in terms of weld width, penetration depth, and reinforcement process profiles and found that the tensile strength was increased. Wan et al. [5] attempted to modify the weld geometry through multi-pass welding with swing-improved TIG for aluminium AA 2219 alloys. It was observed

that the joints with a tensile strength coefficient of 70 % and elongation over 4 % were acquired after weld geometry optimization. Aravind and Das [6] investigated welding aluminium 7075 alloy and found that the maximum welding strength achieved by optimizing the process parameters (100 A current, 60 mm/min welding speed, and 17 lit/min gas flow rate) was 130.27 MPa. Samiuddin et al. [7] investigated on the weldability of the Al-5083 alloy under the influence of different heat inputs (varied from 1 kJ/mm to 2 kJ/mm) in the TIG welding process. Tensile strength 18.26 % of datum strength was lost after welding from base material were compared. Joseph and Muthukumaran [8] investigated optimizing pulsed GTAW welding parameters for AISI 4135 powder metallurgy steel weld using a simulated and genetic algorithm and inferred that peak current of 80 A, base current of 35 A, welding speed 60 mm/min, and gas flow rate of 12 lit/min improved the tensile strength up to 685.31 MPa. Adalarasan and Santhanakumar [9] performed welding experiments on 6061 aluminium alloy based on Taguchi orthogonal L9 array and employed grey relational analysis to study the significance of the welding parameters. Input parameters including arc voltage (17 V to 24 V), current (160 A to 180 A), welding speed (90 mm/min to 110 mm/min), and gas flow rate (9 lit/h to 14 lit/h) were varied to determine the mechanical characteristics; it

was concluded that current has greater significance (47 %) over the mechanical properties followed by arc voltage (35 %). Kanakavalli et al. [10] investigated the effect of welding current, voltage, speed, and bevel angle in joining two dissimilar metals; it was observed that characteristics like tensile strength up to 405.62 MPa and hardness up to 150.4 HV was enhanced for the optimal parameter values of 150 A, 16 V, 0.94 m/min and 45°. Hazari et al. [11] studied the fracture behaviour of AA6082 and AA8011 butt-sweated joint deformation during tensile tests. As the intensity of current increased, the ultimate tensile strength was improved from 90.25 MPa to 170.25 MPa remarkably with a considerable increase in its yield strength. Kumar and Sundarrajan [12] approached Taguchi's technique to optimise pulsed TIG welding process parameters such as pulsed current (70 A to 80 A), base current (40 A to 50 A), welding speed (210 mm/min to 230 mm/min), and pulse frequency (2 Hz to 4 Hz) of AA 5456 aluminium alloy welds for improvement of 10 % to 15 % in mechanical properties. Shunmugasundaram et al. [13] performed friction stir welding on AA5052 with a Taguchi L9 orthogonal experimental array under the influence of tool rotational speed (650 rpm to 850 rpm), welding speed (20 mm/min to 40 mm/min), and tilt angle (1° to 2°). An optimized process parametric condition (tool rotational speed of 850 rpm, the welding speed of 20 mm/min, and the tilt angle of 2°) was found to obtain better mechanical properties in welded joints. ANOVA was performed to determine the percentage influence of the process parameters on the mechanical properties. Signal-to-noise (S/N) ratio analysis can be performed using the options such as smaller the better, nominal the better and larger the better, according to the desired response. The Taguchi method [14] to [17] allows the understanding of the influence of individual parameters on the materials' performance, i.e., microstructure and mechanical properties.

The present study aims to weld the AA5052 alloy through the TIG welding process parameters using the Taguchi method. Process parameters such as current, voltage, and speed were varied during the welding process to study their significance on enhancing the reinforcement form factor (RFF), penetration shape factor (PSF) and hardness. Analysis of variance (ANOVA), S/N ratio analysis, and regression analysis were also performed.

1 MATERIAL AND METHODS

AA5052 aluminium alloy was used in this experimental work as the parent material with plate

thickness of 3.5 mm, length of 100 mm, and width of 100 mm. The parent material was welded with the TIG welding process using ER5356 filler material with a 2.4 mm diameter [18]. The chemical compositions of parent and filler material are listed in Table 1. The mechanical properties of the parent and filler material is given in Table 2. The TIG welding process focuses on the three essential parameters (welding current, voltage, and speed) which are generally considered for controlling weld quality and weldability characteristics [19]. Trials were carried out to select the upper and lower levels of the process parameters. A Taguchi L27 orthogonal array was selected, and the experiments were carried out accordingly. The TIG welding process parameters and their levels are shown in Table 3. The quality characteristics PSF, RFF and hardness of the parent material into the weld were evaluated for all the trials, and then ANOVA was carried out.

The applied criteria for the evaluation of PSF, RFF, and hardness are kept as larger-is-better. PSF defines the ratio of the width of the weld bead to the penetration height of weld. RFF is given by the ratio of weld bead width to reinforcement. An increase of RFF is obvious as the weld bead width decreases while reinforcement increases with heat input.

According to the ANOVA Tables 8 to 10, the input of the welding parameter and their interaction in influencing the characteristic of weld quality is evaluated [20]. The ANOVA also provides an indication of which welding parameters are statistically significant. The optimum welding parameter combination is estimated and proved. Welded specimens were taken, and the metallographic examination was carried out according to the ASTM E3 standard. A schematic illustration of weld bead is shown in Fig. 1. The macrograph of actual bead formation is shown in Fig. 2. The hardness of the welded specimens was measured as per the ASTM 384 standard [20] using a Vickers digital hardness testing machine [21].

Table 1. Chemical composition of the base and filler material

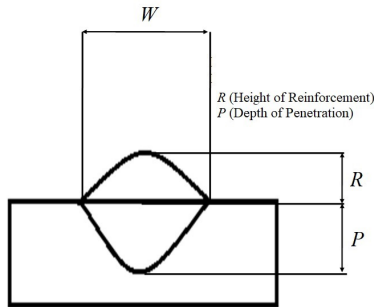
Elements	Si	Mn	Mg	Zn	Al
AA5052-H32	0.1	0.10	3.02	0.025	Bal.
ER 5356	0.052	0.11	3.33	0.069	Bal.

Table 2. Mechanical properties of the base and filler material

Material	Yield strength [MPa]	Tensile strength [MPa]	Hardness [HV]
AA5052-H32	160	230	61
ER 5356	198	295	-

Table 3. Welding parameters

Parameter	Unit	Factor Levels		
		1	2	3
Current	A	40	90	140
Voltage	V	10	14	18
Speed	mm/min	150	200	300



Reinforcement form factor ($RFF = W/R$); Penetration shape factor ($PSF = W/P$)

Fig. 1. Schematic illustration of weld bead



Fig. 2. Macrograph of actual bead formation

2 RESULTS AND DISCUSSION

In the following section, the statistical investigation of the RFF, PSF and hardness, signal-to-noise ratio analysis, analysis of variance, and regression analysis are discussed.

2.1 Statistical Analysis of RFF, PSF, and Hardness

RFF, PSF, and hardness obtained for the different experimental conditions are shown in Table 4. The maximum hardness of 145.3 HV 0.5 is a result of the RFF of 4.49 and PFF of 3.83 under current of 140 A, voltage of 18 V, and speed of 300 mm/min. The plots obtained for the corresponding RFF, PSF, and hardness are shown in Fig. 3. The main effect plot for RFF, PSF, and hardness is displayed for each level of individual parameter. From the RFF plot, it is observed that RFF becomes drastically increased when current is increased from 40 A to 140 A. The RFF is increased with increases in voltage slightly whereas there is only very minimal influence of speed in increasing the

RFF. The PSF plot showed that PSF is decreased when current is increased. PSF is decreased moderately with increases in voltage, whereas there is a only very minimal influence of speed in decreasing the PSF.

From the plot, it is inferred that hardness is increased drastically with increases in the current level, whereas a slight increase of hardness with respect to increases in voltage, and there is no significant increase with increase in speed. Overall, interaction plots show that a current of 140 A and voltage of 18 V have greater tendency to improve the hardness.

2.2 Surface Plot of RFF, PSF and Hardness

The surface plot for RFF, PSF, and hardness with respect to changes in the interaction of current and voltage is shown in Fig. 4. Surface plots with respect to current and voltage are only preferred for analysis since there is no significant influence of speed.

Table 4. RFF, PSF and hardness obtained for the L27 orthogonal array

S. No.	Current [A]	Voltage [V]	Welding speed [mm/min]	RFF	PSF	Hardness
1	40	10	150	2.08	5.7	103.2
2	40	10	200	2.16	5.8	104.5
3	40	10	300	2.1	5.65	108.5
4	40	14	150	2.15	5.62	106.3
5	40	14	200	2.27	5.42	109.5
6	40	14	300	2.39	5.45	111.4
7	40	18	150	2.2	5.82	114.5
8	40	18	200	2.31	5.89	115.2
9	40	18	300	2.26	5.92	116.7
10	90	10	150	2.37	6.13	118.3
11	90	10	200	2.45	6.11	120.4
12	90	10	300	3.16	6.09	122.4
13	90	14	150	3.11	5.82	124.5
14	90	14	200	3.25	5.68	123.8
15	90	14	300	3.26	5.47	126.9
16	90	18	150	3.55	5.59	128.5
17	90	18	200	3.62	5.35	130.5
18	90	18	300	3.59	5.45	132.4
19	140	10	150	4.06	4.87	134.6
20	140	10	200	4.12	4.61	136.5
21	140	10	300	4.15	4.72	137.4
22	140	14	150	4.12	4.66	139.2
23	140	14	200	4.01	4.14	140.3
24	140	14	300	4.39	4.28	141.3
25	140	18	150	4.45	4.25	142.6
26	140	18	200	4.6	4.12	143.2
27	140	18	300	4.49	3.83	145.3

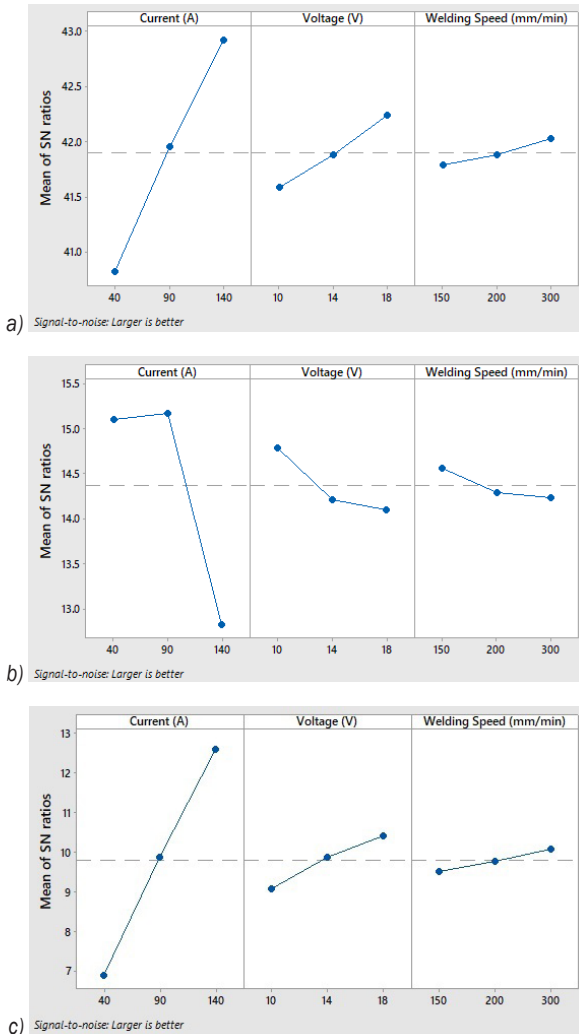


Fig. 3. Main effect plot for a) RFF b) PSF and c) hardness

The surface plot represents the three dimensional (3D) change of RFF, PSF, and hardness. It can be seen from Fig. 4a that the RFF increased drastically with the increase of the current and slightly with respect to changes in voltage. When the current is increased, the voltage is increased proportionally, which in turn deposits a higher amount of filler material for each unit of the weld length. With the high currents applied to each unit, the duration of the welding contributes to an extension of the width of the welding bead.

Fig. 4b shows the PSF decreased with increasing current and voltage. Figure 4c illustrates that the hardness of the fusion zone increased with increasing current and voltage. It is observed that hardness is influenced by high current (140 A) and high voltage (18 V). The increases in welding current and voltage, as well as other variables, were constant; an increase in hardness is evident. Notably, PSF graphs depict

the interaction between current and voltage. Here, the current and voltage increase tends to decrease the PSF.

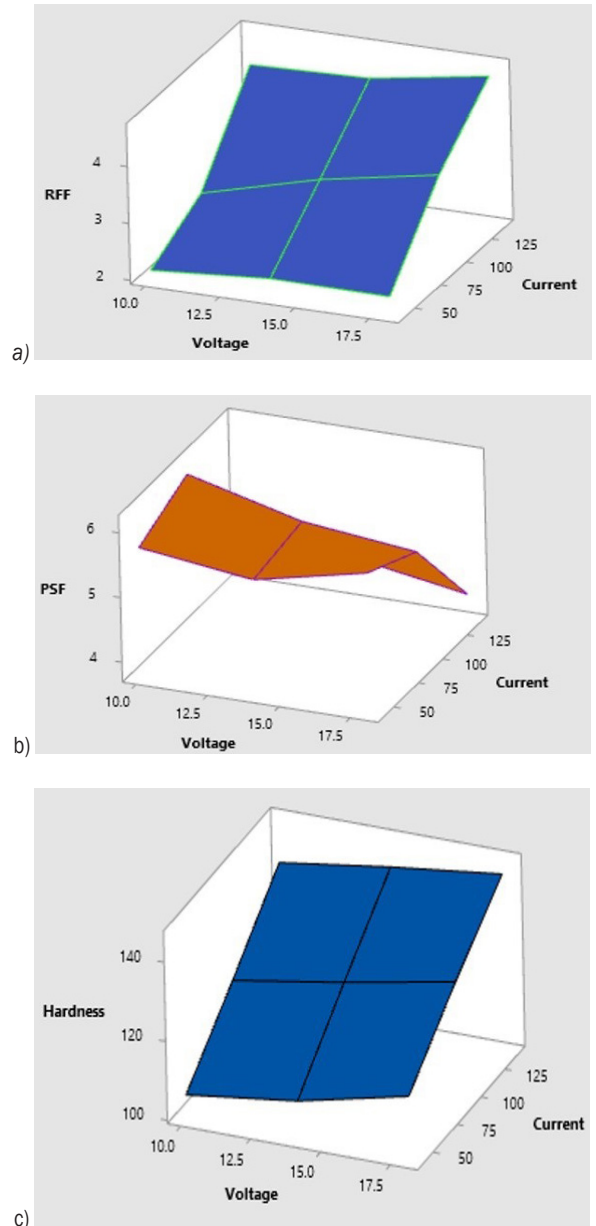


Fig. 4. Surface plots for a) RFF, b) PSF, and c) hardness with respect to change in interaction of current and voltage

2.3 Predicted Plot RFF, PSF and Hardness

The predicted plot for RFF, PSF, and hardness are shown in Fig. 5. Fig. 5a illustrates the predicted points are closed along with the residuals.

Fig. 5b shows that predicted points are scattered along with residuals, and Fig. 5c demonstrates that predicted points are correlated to residuals.

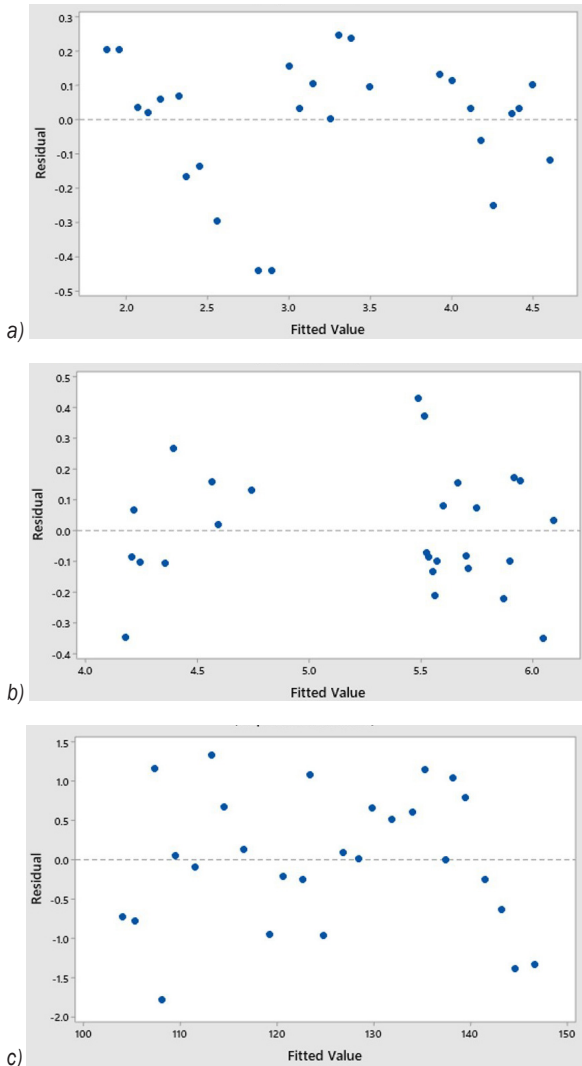


Fig. 5. Predicted plot for the a) RFF, b) PSF, and c) hardness

2.4 Signal-to-Noise Ratio Analysis

The S/N ratio analysis is performed for “larger-is-better” option using Eq. (1), and a response is generated to estimate the influencing order of parameters on hardness. Tables 5 to 7 show the response table for S/N ratios of RFF, PSF, and hardness, respectively.

$$MSD = \frac{1}{n} \sum_{i=1}^n \frac{1}{y_i^2}, \quad (1)$$

where *MSD* is the mean squared deviation, *y_i* the response of *i*th experiment value, and *n* replication number.

The delta value shows the variation in mean within levels, and the delta value is computed through subtracting the smallest from the largest value of the

signal-to-noise ratio. The delta value becomes higher, as there is greater variation of mean values. The factor with the highest delta value has more influence on the dilution and hardness. The delta value indicates the rank of the factors. It is observed from the delta value that current has major significance on RFF, PSF, and hardness, followed by voltage and speed.

Table 5. Response table for S/N ratios of RFF (larger-is-better)

Level	Current [A]	Voltage [V]	Speed [mm/min]
1	6.893	9.066	9.513
2	9.876	9.875	9.766
3	12.590	10.417	10.079
Delta	5.697	1.351	0.565
Rank	1	2	3

Table 6. Response table for S/N ratios of PSF (larger-is-better)

Level	Current [A]	Voltage [V]	Speed [mm/min]
1	15.11	14.79	14.57
2	15.17	14.21	14.29
3	12.82	14.10	14.24
Delta	2.35	0.69	0.33
Rank	1	2	3

Table 7. Response table for S/N ratios of hardness (larger-is-better)

Level	Current [A]	Voltage [V]	Speed [mm/min]
1	40.82	41.58	41.78
2	41.95	41.88	41.88
3	42.92	42.24	42.03
Delta	2.10	0.65	0.24
Rank	1	2	3

2.5 Analysis of Variance

The analysis of variance is performed for the significance level 5 % and confidence level 95% to evaluate the influence of various input process parameters on the RFF, PSF, and hardness, which is shown in Tables 8 to 10. The significance level indicates the confidence of repeatability of the experimental results. The percentage significance of the factors are determined and included in the last column. For RFF, current has the higher percentage of contribution (89.5 %) compared to voltage (5.13 %) and speed (0.77 %). For PSF, current also has the higher percentage of contribution (61.15 %) compared to voltage (5.27 %) and speed (1.13 %) and hardness; current also has greater influence (89.89%) compared to voltage (8.48 %) and speed (1.15 %).

Table 8. Analysis of variance for RFF versus current, voltage, speed

Source	Degree of freedom	Sequential Sum of square	Adjusted Sum of square	Adjusted mean square	F	% Contribution
Current	1	18.9523	18.9523	18.9523	455.77	89.5
Voltage	1	1.0854	1.0854	1.0854	26.10	5.13
Speed	1	0.1624	0.1624	0.1624	3.91	0.77
Error	23	0.9564	0.9564	0.0416		4.52
Total	26	21.1565				100

Table 9. Analysis of variance for PSF versus current, voltage, speed

Source	Degree of freedom	Sequential Sum of square	Adjusted Sum of square	Adjusted mean square	F	% Contribution
Current	1	7.7224	7.7224	7.7224	43.33	61.15
Voltage	1	0.6651	0.6651	0.6651	3.73	5.27
Speed	1	0.1422	0.1422	0.1422	0.80	1.13
Error	23	4.0995	4.0995	0.1782		32.46
Total	26	12.6293	7.7224	7.7224		100

Table 10. Analysis of variance for PSF versus current, voltage, speed

Source	Degree of freedom	Sequential Sum of square	Adjusted Sum of square	Adjusted mean square	F	% Contribution
Current	1	4068.02	4068.02	4068.02	4277.52	89.89
Voltage	1	383.64	383.64	383.64	403.40	8.48
Speed	1	52.02	52.02	52.02	54.70	1.15
Error	23	21.87	21.87	0.95		0.48
Total	26	4525.56	4068.02	4068.02		100

2.6 Regression Analysis with Confirmation Experiments

The regression equations are generated as per the influence of parameters indicated in the analysis of variance [22]. The regression equations for the RFF, PSF, and hardness are given in Eqs. (2) to (4), respectively.

$$RFF = 0.235 + 0.020522 I + 0.0614 U + 0.001238 v_w, \tag{2}$$

$$PSF = 7.356 - 0.01310 I - 0.0481 U - 0.00106 v_w, \tag{3}$$

$$Hardness = 77.05 + 0.30067 I + 1.1542 U + 0.02235 v_w, \tag{4}$$

where *I* is current parameter, *U* voltage parameter and *v_w* welding speed parameter.

These regression models relate the *RFF*, *PSF*, and *Hardness* of the welded specimens with the parameters such as current, voltage, and speed. In Eqs. (2) and (4), the parameter prefixed with the plus (+) sign indicates that increasing the level of that parameter increases *RFF* and *Hardness*. In Eq. (3), a minus (-) sign denotes that enhancing parameter level declines the responses. The sufficiency of the developed regression model has been confirmed by the confirmation experiments for *RFF*, *PSF*, and *Hardness*

of the welded specimens, shown in Tables 10 to 12. The new set of parametric conditions is incorporated in the developed model, and the determined *RFF*, *PSF*, and *Hardness* are checked with the experimental values for similar parametric conditions. The error [%] between model and experimental values has been computed, and it lies within the 5 % range. This, in turn, indicates that the developed regression model has greater adequacy in predicting the *RFF*, *PSF*, and *Hardness* of the welded specimens by connecting it with the process parameters.

Table 10. Regression analysis and confirmation experiments (RFF)

Current [A]	Voltage [V]	Speed [mm/min]	Experimental	Regression	Error [%]
90	10	150	2.52	2.61	3.5
120	14	200	3.86	3.80	1.5
150	18	300	4.61	4.78	3.6

Table 11. Regression analysis and confirmation experiments (PSF)

S. No.	Current [A]	Voltage [V]	Speed [mm/min]	Experimental	Regression	Error [%]
1	90	10	150	5.394	5.537	2.6
2	120	14	200	4.923	4.898	0.5
3	150	18	300	4.443	4.205	4.9

Table 12. Regression analysis and confirmation experiments (Hardness)

S. No.	Current [A]	Voltage [V]	Speed [mm/min]	Experimental	Regression	Error [%]
1	90	10	150	123.21	119.00	3.5
2	120	14	200	136.96	133.75	2.4
3	150	18	300	148.21	149.36	0.7

2.7.1 Microstructural Analysis

The microstructure of the AA5052 aluminium alloy weldment cross-section highlights the parent material (PM), fusion zone (FZ), and heat-affected zone (HAZ) were taken using an inverted metallurgical optical microscope. Fig. 6 shows an α -aluminium matrix in the PM. In Fig. 7, defects such as void, crack, and unbounded regions in and around the weld region for the weld are not observed [23] and [24]. In tungsten inert gas welds, grain development is evident on the weld site (fusion zone). This reveals elongated cellular dendritic grains with coarse Mg_2Si particles distributed in the α -aluminium matrix. The coarsening of grain reduces the strength of the fusion zone. The dendritic structure formed in the fusion zone depends on the cooling rate. As the heat input increased during the welding process, the cooling rate will be lower, which will result in the formation of coarser dendrites.

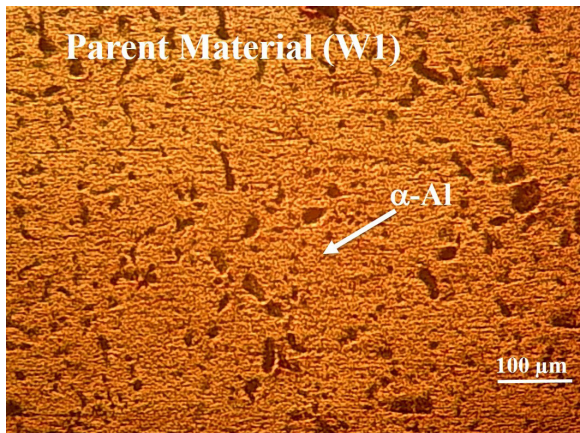
**Fig. 6.** Parent materials

Fig. 8 shows the transition zone, i.e., fusion zone to the heat-affected zone for the three experimental conditions. The left portion of the microstructure indicates the dendritic formation in the fusion zone, and the right portion of the microstructure reveals the formation of equiaxed grains at the HAZ, which is commonly observed in the strain-hardened 5052-H32 alloy.

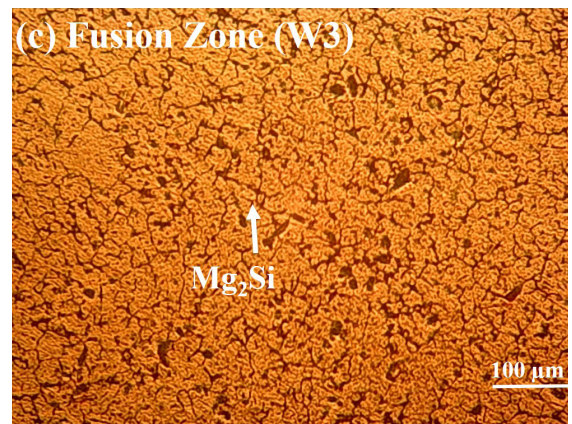
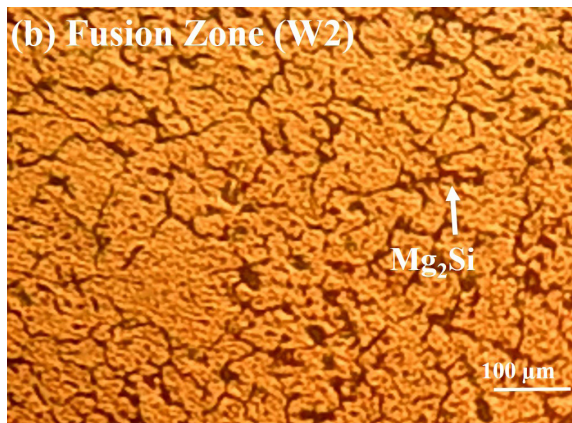
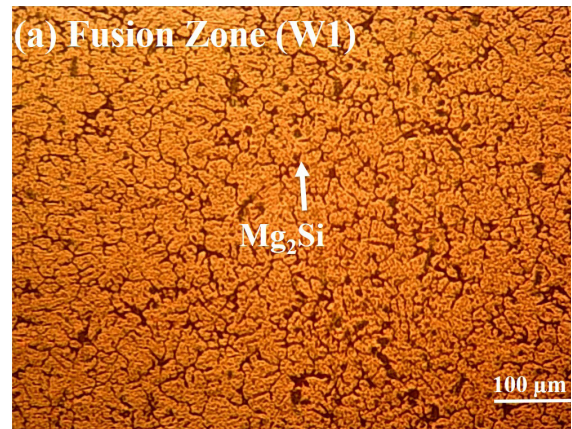
**Fig. 7.** Fusion zone of the different weldments
a) 90 A, 10 V, 150 mm/min b) 120 A, 14 V, 200 mm/min,
and c) 150 A, 18 V, 300 mm/min

Fig. 9 shows the phase variation in the heat affect zone. This results from the high thermal conductivity of aluminium alloys, specifically at lower welding current, which leads to high thermal losses transverse in the welding directions. Fig. 10 presents the influence of the welding current (90 A, 120 A, and 150 A) on the phase variation (16.17 μ m, 9.53 μ m, and 7.54 μ m) and grain size (102.014 μ m, 116.429 μ m,

and $126.89 \mu\text{m}$), respectively. As welding current increases, phase variation also decreases.

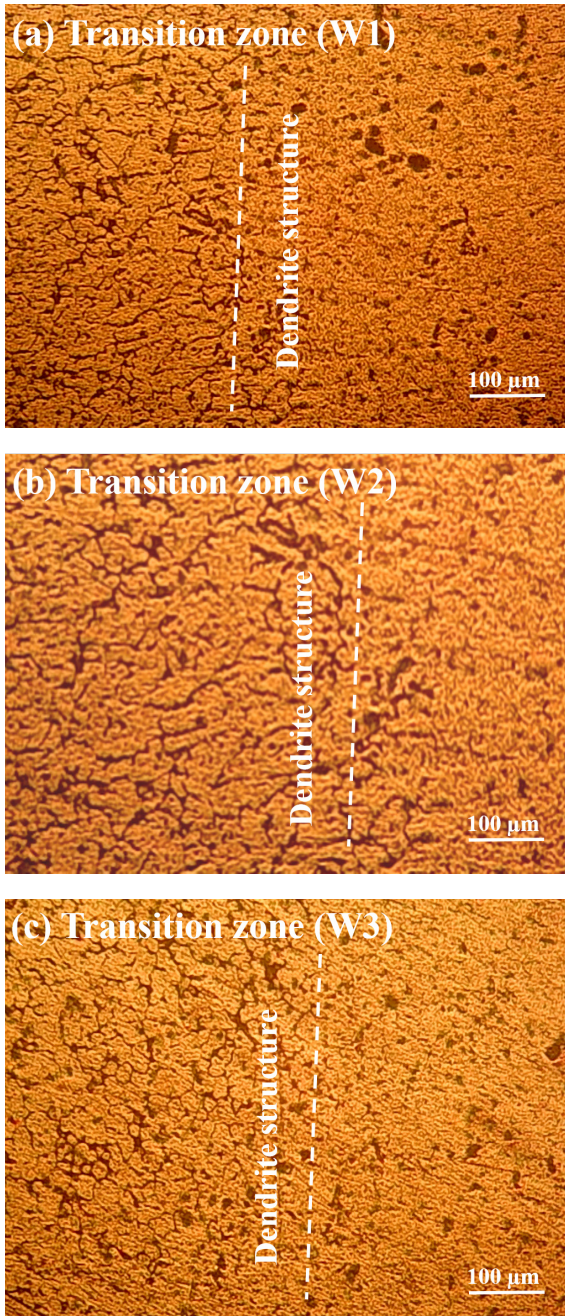


Fig. 8. Transition zone of the different weldments a) 90 A, 10 V, 150 mm/min b) 120 A, 14 V, 200 mm/min and c) 150 A, 18 V, 300 mm/min

2.7.2 Hardness Testing

The hardness profiles are studied in cross-section of weldments produced at confirmation experimental



Fig. 9. Transition zone of the different weldments with partially phase variations a) 90 A, 10 V, 150 mm/min b) 120 A, 14 V, 200 mm/min, and c) 150 A, 18 V, 300 mm/min

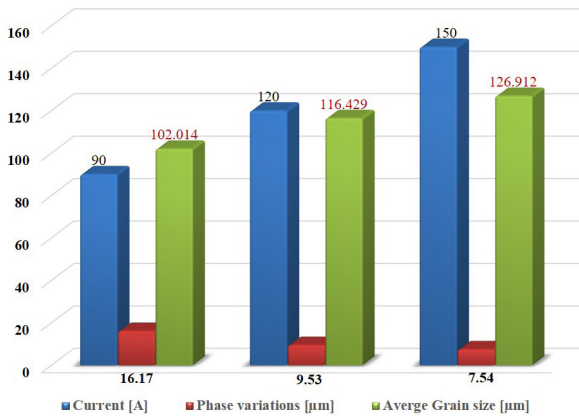


Fig.10. Influence of welding current

conditions, Fig. 11. Hardness is found lowest at the base material whereas the heat-affected zone is having relatively higher hardness than base metal. There is further increase in the hardness upon reaching the fusion zone. Overall, hardness gets increased from base metal towards the fusion zone. This trend across the zones is due to rapid cooling rate occurring in the HAZ and fusion zones. In addition, the higher hardness in the fusion zone owing to formation of Mg_2Si with a fine grain structure in weldment. Similar trend of microhardness across the different zones of the weldment is reported elsewhere [25].

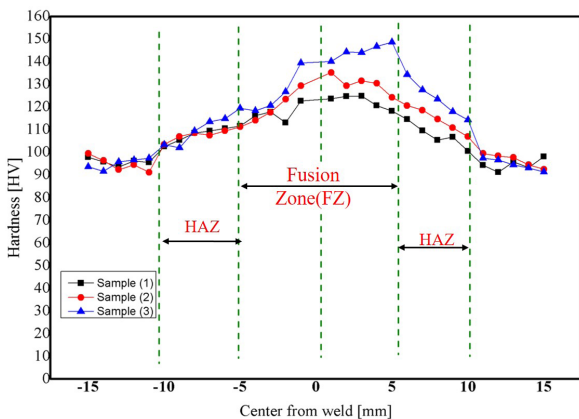


Fig. 11. Hardness of the different zones welded for confirmation experiments

3 CONCLUSION

- A study was conducted to determine appropriate welding process and produce a set of welding parameters for components used in marine applications, automobile structural applications, and chemical processing industries.

- AA5052 was successfully welded using tungsten inert gas welding process under L27 experimental array using Taguchi's method. Welding experiments revealed that, the maximum hardness of 145.3 HV 0.5 is resulted for the RFF of 4.49 and PFF of 3.83 under the current (140 A), voltage (18 V) and speed (300 mm/min).
- The RFF gets increased drastically when current is increased from 40 A to 140 A. PSF gets decreased moderately with increase in voltage whereas there is only very minimal influence of speed in decreasing the PSF. The hardness gets increased drastically with increase in current level whereas there is slight increase of hardness with respect to increase in voltage and there is no significant increase with increase in speed. In overall, interaction plots evident that current of 140 A and voltage of 18 V has greater tendency to improve the hardness.
- S/N ratio and ANOVA showed that current has the major significance on RFF, PSF and hardness followed by voltage and speed. Regression analysis evident that developed model has greater adequacy in predicting the RFF, PSF and hardness of the welded specimens by connecting it with the process parameters.
- Defects such as void, crack, and unbounded regions in and around the weld region for the weld is not observed in the microstructure. The grain development is evident on the fusion zone. This reveal elongated cellular dendritic grains with coarse Mg_2Si particles distributed in the α -aluminium matrix.
- Hardness profile for the specimen welded at confirmation experimental conditions showed that hardness was found higher at fusion zone followed by heat-affected zone and base metal.

4 REFERENCES

- Balaram Naik, A., Chennakeshava Reddy, A. (2018). Optimization of tensile strength in TIG welding using Taguchi method and analysis of variance (ANOVA). *Thermal Science and Engineering Progress*, vol. 8, p. 327-339, DOI:10.1016/j.tsep.2018.08.005.
- Sathishkumar, D., Daniel Das, A. (2021). Investigations on effect of process parameters on GTAW of aluminium alloy welding using full factorial design technique. *Materials Today: Proceedings*, vol. 37, part 2, p. 621-626, DOI:10.1016/j.matpr.2020.05.624.
- Shanavas, S., Dhas, J.E.R., Murugan, N. (2018). Weldability of marine grade AA 5052 aluminium alloy by underwater friction stir welding. *The International Journal of Advanced*

- Manufacturing Technology*, vol. 95 p. 4535-4546, DOI:10.1007/s00170-017-1492-6.
- [4] Denykui, Z., Wang, G., Wu, A., Zhao, Y., Li, Q., Liu, X., Meng, D., Song, J., Zhang, Z. (2018). Study on the inconsistency in mechanical properties of 2219 aluminium alloy TIG-welded joints. *Journal of Alloys and Compounds*, vol. 777, p. 1044-1053, DOI:10.1016/j.jallcom.2018.10.182.
- [5] Wan, Z., Meng, D., Zhaom Y., Zhang, D., Wang, Q., Shan, J., Song, J., Wang, G., Wu, A. (2021). Improvement on the tensile properties of 2219-T8 aluminium alloy TIG welding joint with weld geometry optimization. *Journal of Manufacturing Processes*, vol. 67, p. 275-285, DOI:10.1016/j.jmapro.2021.04.062.
- [6] Aravind, S., Das, A.D. (2020). An examination on GTAW samples of 7-series aluminium alloy using response surface methodology. *Materials Today*, vol. 37, no. 4, p. 1234-1248, DOI:10.1016/j.matpr.2020.05.623.
- [7] Samiuddin, M., Li, J., Taimoor, M., Siddiqui, M., Siddiqui, S.U., Xiong, J. (2020). Investigation on the process parameters of TIG-welded aluminium alloy through mechanical and microstructure characterization. *Defence Technology*, vol. 17, no. 1, DOI:10.1016/j.dt.2020.06.012.
- [8] Joseph, J., Muthukumar, S. (2016) Optimization of pulsed current GTAW process parameters for sintered hot forged AISI 4135 P/M steel welds by simulated annealing and genetic algorithm. *Journal of Mechanical Science and Technology*, vol. 30, p. 145-155, DOI:10.1007/s12206-015-1218-3.
- [9] Adalarasan, R., and Santhanakumar, M., (2015) Parameter design in fusion welding of AA 6061Aluminium alloy using desirability grey relational analysis (DGRA) method. *Journal of The Institution of Engineers (India): Series C*, vol. 96, p. 57-63. DOI:10.1007%2Fs40032-014-0128-y.
- [10] Kanakavalli, P.B., Navaneeth Babu, B., Vishnu Sai, Ch.P.N. (2019). A hybrid methodology for optimizing MIG welding process parameters in joining of dissimilar metals. *Materials Today: Proceedings*, vol. 23, p. 507-512, DOI:10.1016/j.matpr.2019.05.396.
- [11] Hazari, H.R., Balubai, M., Suresh Kumar, D., Ahsan Ul Haq, (2019). Experimental investigation of TIG welding on AA 6082 and AA 8011. *Materials Today: Proceedings*, vol. 19, p. 818-822, DOI:10.1016/j.matpr.2019.08.137.
- [12] Kumar, A., Sundararajan, S. (2009). Optimization of pulsed TIG welding process parameters on mechanical properties of AA 5456 Aluminium alloy weldments. *Materials and Design*, vol. 30, no. 4, p. 1288-1297, DOI:10.1016/j.matdes.2008.06.055.
- [13] Shunmugasundaram, M., Praveen Kumar, A., Ponraj Sankar, L., Sivasankar, S. (2020). Optimization of process parameters of friction stir welded dissimilar AA6063 and AA5052 aluminum alloys by Taguchi technique. *Materials Today: Proceedings*, vol. 27, p. 871-876, DOI:10.1016/j.matpr.2020.01.122.
- [14] Vora, J., Patel, V.K., Srinivasan, S., Chaudhari, R., Pimenov, D.Y., Giasin, K., Sharma, S. (2021). Optimization of activated tungsten inert gas welding process parameters using heat transfer search algorithm: With experimental validation using case studies. *Metals*, vol. 11, art. ID 981, DOI:10.3390/met11060981.
- [15] Srirangan, A.K., Paulraj, S. (2016). Multi-response optimization of process parameters for TIG welding of Incoloy 800HT by Taguchi grey relational analysis. *Engineering Science and Technology*, vol. 19, no. 2, p. 811-817, DOI:10.1016/j.jestch.2015.10.003.
- [16] Kasirajan, G., Sathish Rengarajan , Ashok kumar ,R., Raghav, G.R., Rao,V.S., and Nagarajan, K.J. (2020). Tensile and wear behaviour of friction stir welded AA5052 and AA6101-T6 aluminium alloys: effect of welding parameters, Metallurgical Research and Technology, vol. 117, no. 4, art. ID 405, DOI:10.1051/metal/2020039.
- [17] Sathish, T., Tharmalingam, S., Mohanavel, V., Ashraff Ali, K., Karthick, S., Ravichandran, A., Rajkumar, M., Sivanraju (2021). Weldability Investigation and Optimization of Process Variables for TIG-Welded Aluminium Alloy (AA 8006). *Advances in Material Science and Engineering*, art. ID 2816338, DOI:10.1155/2021/2816338.
- [18] Dhanaraj, A.P., Kumarasamy, S. (2021). Mechanical properties and metallurgical characterization of FSPed TIG and TIG welded AA5052-H32/AA5083-H111 dissimilar aluminium alloys. *Metallurgical Research and Technology*, vol. 118, art. ID 304, DOI:10.1051/metal/2021005.
- [19] Safari, M., Mostaan, H. (2016). Experimental investigation of the effects of process parameters on the strength of eutectoid steel (AISI 1075) sheet resistance spot welds. *Metallurgical Research and Technology*, vol. 113, p. 305-318, DOI:10.1051/metal/2016005.
- [20] Sudhakar,R., Sivasubramanian, R., Yoganandh, J. (2017), Effect of automated MIG welding process parameters on ASTM A 106 Grade B pipe weldments used in high-temperature applications. *Materials and Manufacturing Processes*, vol. 33, no. 7, p. 749-758, DOI:10.1080/10426914.2017.1401719.
- [21] Skariya, P.D., Satheesh, M., Dhas, J.E.R. (2018). Optimizing parameters of TIG welding process using grey wolf optimization concerning 15CDV6 steel. *Evolutionary Intelligence*, vol. 11, p. 89-100, DOI:10.1007/s12065-018-0161-5.
- [22] Radhika, N., Raghu, R. (2017). Investigation on mechanical properties and analysis of dry sliding wear behavior of Al LM13/AlN metal matrix composite based on Taguchi's technique. *Journal of Tribology*, vol. 139, no. 4, art. ID 041602, DOI:10.1115/1.4035155.
- [23] Ebrahimzadeh, I., Sadeghi, B., Maddahi, H. (2019). Welding of thin sheet of Al5456 aluminium alloy by using GTA and GMA welding process. *Materials Research Express*, vol. 6, vol. 6, DOI:10.1088/2053-1591/ab0d48.
- [24] Hagenlocher, C., Wellera, D., Weber, R., Graf, T. (2019), Reduction of the hot cracking susceptibility of laser beam welds in Al-Mg-Si alloys by increasing the number of grain boundaries. *Science and Technology of Welding and Joining*. vol. 24, no. 4, p. 313-319, DOI:10.1080/13621718.2018.1534775.
- [25] Abioye,T.E., Zuhailawati,H., Aizad, S., Anasyida, A.S. (2019). Geometrical, microstructural and mechanical characterization of pulse laser welded thin sheet 5052-H32 aluminum alloy for aerospace applications. *Transactions of Nonferrous Metals Society of China*, vol. 29, no. 4, p. 667-679, DOI:10.1016/S1003-6326(19)64977-0.